Article (refereed) - postprint

Wang, Qingqing; Zhang, Qi; Ma, Zhiqiang; Ge, Baozhu; Xie, Conghui; Zhou, Wei; Zhao, Jian; Xu, Weiqi; Du, Wei; Fu, Pingqing; Lee, James; Nemitz, Eiko; Cowan, Nicholas; Mullinger, Neil; Cheng, Xueling; Zhou, Libo; Yue, Siyao; Wang, Zifa; Sun, Yele. 2019. **Temporal characteristics and vertical distribution of atmospheric ammonia and ammonium in winter in Beijing**.

Temporal characteristics and vertical distribution of atmospheric ammonia and ammonium in winter in Beijing

Qingqing Wang[a,b,c], Qi Zhang[b*], Zhiqiang Ma[d], Baozhu Ge[a], Conghui Xie[a,c], Wei Zhou[a,c], Jian Zhao[a,c], Weiqi Xu[a,c], Wei Du[a], Pingqing Fu[e], James Lee[f], Eiko Nemitz[g], Nicholas Cowan[g], Neil Mullinger[g], Xueling Cheng[a], Libo Zhou[a], Siyao Yue[a,c], Zifa Wang[a], Yele Sun[a,c*]

[a] State Key Laboratory of Atmospheric Boundary Layer Physics and Atmospheric Chemistry, Institute of Atmospheric Physics, Chinese Academy of Sciences, Beijing 100029, China

[b] Department of Environmental Toxicology, University of California, Davis, CA 95616, USA

[c] University of Chinese Academy of Sciences, Beijing 100049, China

[d] Institute of Urban Meteorology, China Meteorological Administration, Beijing 100089, China

[e] Institute of Surface-Earth System Science, Tianjin University, Tianjin 300072, China

[f] National Centre for Atmospheric Science, University of York, York, UK

[g] Centre for Ecology & Hydrology, Bush Estate, Penicuik, Midlothian, EH26 0QB, UK

Correspondence: Qi Zhang (dkwzhang@ucdavis.edu); Yele Sun (sunyele@mail.iap.ac.cn)

ABSTRACT

To understand the temporal characteristics and vertical distributions of ammonia (NH_3) and ammonium (NH_4) in urban Beijing, we conducted ground-based and tower-based measurements of gaseous NH_3 and submicron aerosol composition. The average mixing ratio of NH_3 was 16.5 ± 7.4 ppb, ranging from 3.8 to 36.9 ppb. Gas-to-particle partitioning of NH_x (= NH_3 + NH_4) played a significant role on NH_3 concentration as the molar ratio of NH_3 to NH_x decreased as a function of NH_4 concentration. The NH_3 concentrations increased as a function of PM_1 at lower levels (< 125 μg m^{-3}), but remained relatively constant at higher PM and NH_4 levels, indicating an enhanced gas-to-particle conversion of NH_3 during highly polluted conditions. The potential sources of NH_x were found to include fossil fuel combustion and biomass burning. Regional transport could also play an important role on NH_3 concentration during the formation stage of haze episodes due to particle-to-gas conversion. Four distinctive types of vertical profiles (87% of the time) of both NH_3 and fine particle light extinction coefficient (b_{ext}) were observed and they were associated with well-mixed atmosphere, fast accumulation of local emissions, regional transport aloft, and the formation of low urban boundary layer, respectively. However, the vertical profiles of NH_3 typically (96% of the time) showed a more homogeneous characteristic than those of b_{ext} below 260 m, except periods with both strong temperature inversion and large aerosol gradient, the formation of urban boundary layer shall cause a significant transition in the vertical distribution of NH_3 below 260 m. During highly polluted situations (PM_1 > 125 μg m^{-3}), the strong effect of gas-to-particle partitioning of NH_x sometimes (7% of the time) caused opposite trends in vertical profiles of NH_3 and b_{ext}.

Key words:

Ammonia, NH_x, Vertical distribution, Extinction coefficient, Beijing

1. Introduction

NH_3 plays an important role in urban air pollution processes, such as the formation of secondary inorganic aerosol species of SNA (sulfate + nitrate + ammonium) (Wang et al., 2011). Other fine particle chemical species, e.g., organics, chloride, nitrate, sulfate and black carbon are relatively well understood during severe haze episodes in China (Sun et al., 2013; Wang et al., 2015; Zhang et al., 2015), the evolution mechanisms for ammonium remain poorly characterized. In addition, NH_x (= NH_3 + NH_4) control has been found playing an effective role on reduction of $PM_{2.5}$ pollution (Giannadaki et al., 2018; Guo et al., 2018; Pozzer et al., 2017). NH_3 is mainly released from agricultural activities and breeding industry on a global scale (Van Damme et al., 2018), however, the sources for the high level of NH_3 observed in urban areas remain a controversial topic (Zhang et al., 2017) as there are little local contributions from the two sources mentioned above. Traffic emission has been reported as an important source for NH_3 in urban areas (Elser et al., 2018). Coal combustion and biomass burning, which are major contributors to severe haze pollution in Beijing, have been found to emit significant amount of NH_3 (Li et al., 2016). Some point sources, e.g., wastewater treatment plants, can also emit NH_3 (Van Damme et al., 2018). The sources for NH_3 were studied via N isotopic ratios in nitrate and simulated NH_3 in Pan et al. (2016; 2018), and via direct measurement of NH_3 in Chang et al. (2015), however, the relationship between ammonium and NH_3 was not further discussed. NH_3 concentration was usually found depending exponentially on temperature (Chang et al., 2015), especially during winter time (Teng et al., 2017), indicating a significant effect of gas-particle partitioning on the concentration of NH_3. The uncertainties of ammonia emissions, together with the huge variations in the relationship between emissions and ambient concentrations of NH_3, are causing difficulties in abating NH_4 levels. Thus, it is worthwhile to study the sources and

evolution mechanisms for NH_x via simultaneous measurement of both gaseous NH_3 and particulate ammonium, especially in severely polluted megacities that suffer high level of NH_x (Wang et al., 2015).

The complex vertical evolution of air pollutants is attracting attention due to its strong influence on the accurate prediction of air quality models (Wang et al., 2014). Regional transport usually affected air pollution in urban areas initially above the urban canopy, which could be observed based on the vertical distribution of air pollutants (Sun et al., 2015; Wang et al., 2018). The weekly vertical distribution of ammonia (NH_3) measured at 16 different heights on the Beijing 325 m meteorological tower (BMT) showed that NH_3 was rich during all seasons below 320 m (Zhang et al., 2018). High time resolution method for vertically resolved studies shows that NH_3 concentration at higher altitudes appears to be driven by transport while that at lower altitudes is strongly influenced by surface emissions and boundary layer height (Tevlin et al., 2017). To date, the vertical profiles of NH_x at urban area in highly polluted megacities in China have rarely been studied.

In this study, highly time-resolved measurements of gaseous NH_3 were conducted at ground site, and the vertically resolved measurements of NH_3 and fine particle extinction coefficient (b_{ext}) were performed from ground level to 260 m on the BMT in November and December 2016. In addition, simultaneous real-time measurements of ammonium in PM_1 particles were conducted at the ground level and 260 m from the tower, along with measurements of the other PM_1 species (i.e., organics, sulfate, nitrate, chloride, and BC) and trace gases (i.e., CO, SO_2, O_3 and nitrogen oxides). Our goals are to elucidate the vertical evolution mechanisms of NH_x and the potential sources for NH_3 within urban boundary layer (UBL) during wintertime in Beijing.

2. Experimental methods

2.1. Sampling site

All measurements were conducted at an urban site between the 3rd and 4th ring road in Beijing located at the Tower Branch of Institute of Atmospheric Physics (TBIAP, 39°58′N, 116°22′E; elevation: 49 m ASL), Chinese Academy of Sciences from November 16 to December 10, 2016. The site is surrounded by roads, expressways, gas stations, residential areas, park, commercial buildings, and restaurants (Fig. 1).

2.2. Ground measurements

NH_3 at ground level was measured using an online LGR ammonia analyzer (DTL-100, Los Gatos Research, California) (Baer et al., 2002) at a time resolution of about 50 s (Location B; Fig. 1). Meng et al. (2018) reported that there was a lag in the results of the LGR ammonia analyzer, and hourly average could reduce this influence. NH_3 measured by the LGR ammonia analyzer tracked well with the measurement at 102 m on the BMT from an open path quantum cascade-laser (QCL)-based NH_3 sensor (Aerodyne Research Inc., USA) using a 3 m fast-response counter-flow impactor inlet, with R^2 = 0.70, *slope* = 0.89 (Fig. S1). Note that a slight time lag of a few seconds was observed between the two measurements. However, the water vapor measured at 50 s resolution by the LGR ammonia analyzer compared extremely well with that measured at 2 s resolution from a ground meteorological station (R^2 = 0.99, slope = 1.19; Fig. S1), and the water vapor and NH_3 measured by the LGR ammonia analyzer were also highly consistent, indicating that the time lag between the LGR ammonia analyzer and the QCL-based NH_3 sensor can be ignored.

Gas analyzers (Thermo Scientific) were deployed from a nearby container (Location C; Fig. 1)

to measure NO/NO_y (Model 42i), CO (Model 48i), O_3 (Model 49i), and SO_2 (Model 43i) simultaneously. CO_2 at 8 m above the ground were measured from the tower using a LI-7500 CO_2/H_2O infrared gas analyzers (LI-COR, Inc., Nebraska, USA) on the BMT (Liu et al., 2015).

At the rooftop of a two-story building (~ 8 m high) (Location A; Fig. 1), non-refractory submicron aerosol (NR-PM_1) species, including organics (Org), sulfate (SO_4), nitrate (NO_3), ammonium (NH_4) and chloride (Chl) were measured by an Aerodyne High-Resolution Time-of-Flight Aerosol Mass Spectrometer (AMS hereafter); BC was measured by a 7-wavelength aethalometer (AE33, Magee Scientific Corp.); extinction coefficients of dry fine PM_1 at 630 nm by a CAPS particle single-scattering albedo monitor (CAPS PM_{SSA}, Aerodyne Research Inc.). The organic aerosol spectral matrices of the AMS were analyzed by Positive Matrix Factorization (PMF) to resolve 6 organic aerosol (OA) factors (Xu et al., 2018), i. e., a fossil-fuel-related OA (FFOA), a cooking OA (COA), a biomass burning OA (BBOA), an oxidized POA (OPOA), an oxygenated OA (OOA), and an aqueous-phase OOA (aq-OOA). Measurements of NH_3 and PM_1 chemical species at ground level were extended to December 22 2016.

2.3. Measurements at 260 m above the ground

Simultaneous measurements of BC, CO, O_3, and SO_2 were conducted at 260 m on the tower using the same type of instruments as those used for the ground observations except that NR-PM_1 was measured with an Aerodyne Aerosol Chemical Speciation Monitor (ACSM) (Sun et al., 2015). The ACSM had been deployed in parallel with the AMS through the same sampling inlet during December 14 to 16, 2016, and the R^2 for the NR-PM_1 species comparisons between the two instruments were 0.97, 0.98, 0.99, 0.99, and 0.98, respectively for Org, SO_4, NO_3, NH_4, and Chl.

High correlation for parallel sampling comparisons of BC and precursor gases with the same model of instruments for measurement at the two heights were also confirmed. b_{ext} (λ = 630 nm) of $PM_{2.5}$ at 260 m was measured by a CAPS particle extinction monitor (CAPS-PM_{ext}, Aerodyne Research Inc.).

2.4. Vertically resolved measurements

A container suspended from a cable car style lift system installed on the BMT was used for vertically resolved measurements at a constant moving speed of ~ 8 m min^{-1}. The ammonia analyzer and a Photo-Acoustic Extinctiometer (PAX, Droplet Measurement Technologies, Inc.) were placed inside the container for measurements of NH_3 and light extinction coefficient at λ = 870 nm of $PM_{2.5}$, respectively. All instruments were powered by Uninterrupted Power Supply, and the vertically resolved measurements were performed between the ground level and aloft about every 4 h during daytime (260 m) and every 6 h during nighttime (240 m) for safety; for the remainder of the time the instruments provided ground measurements, which was similar to the arrangements reported in Wang et al. (2018). In total, 50 sets of vertical profiles (VPs) for b_{ext} (VPs_b_{ext}) and NH_3 (VPs_NH_3) were obtained. Due to the interruption of power supply, 4 VPs_NH_3 were incomplete. Wind speed (WS), wind direction (WD), relative humidity (RH), and temperature (T) at 15 different heights (8, 15, 32, 47, 63, 80, 100, 120, 140, 160, 180, 200, 240, 280, and 320 m) were measured on the BMT.

3. Results and discussion

3.1. Overview of pollution levels

The average mass concentration of PM_1 was 83.3 ± 80.3 μg m^{-3} (Table S1) from November 16 to December 10, with organics, nitrate, sulfate, ammonium, chloride, and black carbon accounted for on average 39.8%, 19.6%, 16.3%, 10.0%, 7.3%, and 7.0%, respectively, indicating a high level of

aerosol pollution in urban Beijing. The average NH_3 mixing ratio during this study was 16.5 ± 7.4 ppb (12.3 ± 5.5 μg m^{-3}), higher than the values previously observed in Shanghai (about 5 ppb in winter and autumn) (Chang et al., 2015) and in winter 2007 in Beijing (5.5 μg m^{-3}), lower than the level observed at a rural site (36.2 ppb) and in urban Beijing in summer 2007 (25.4 μg m^{-3}) (Shen et al., 2011), and was less than 1/10 of those observed in tunnel studies (Chang et al., 2015; Liu et al., 2014). Compared with the results in the heating season of 2012 (Wang et al., 2015), SO_2 was lower by more than 50%. However, CO, NO, NO_2 were at comparable levels, suggesting similar intensity of traffic emission but a significant reduction of coal combustion emission. High values of O_3 could be observed both at daytime and nighttime with low PM_1 mass loadings, indicating that the high background of NO_x and VOCs in Beijing (Fig. 2). High level of O_3 and low levels of other pollutants typically appeared when the northwest wind prevailed (Fig. 2). Low values of O_3 during high pollution episodes were relevant to the lower solar radiation and weak oxidation of atmospheric condition, and high NO that titrated O_3 substantially as the diurnal cycle of O_3 was generally in accordance with that of solar radiation (Wang et al., 2015), and was opposite to those of NO_x, NO_2, and SO_4 (Fig. S2). High RH generally coincided with highly polluted episodes, which is a common feature for severe haze in Beijing (Sun et al., 2014b; Sun et al., 2012; Sun et al., 2013). High f_{NH3} (= NH_3 / NH_x in molar concentrations) appeared during low pollution situations (Fig. 2f) partly due to low RH which tended to inhibit the transformation of NH_3 to ammonium.

The diurnal cycle of NH_x was similar to those of Chl, BC, CO, and NO, suggesting coal combustion and traffic were two important sources for NH_3 and NH_4. Both NO and CO_2 peaked at 8:00, indicating that traffic emission was an important source of CO_2 in our study. The diurnal profile of SO_2, a gas species dominantly from coal combustion emissions, generally agreed well with that of

NH_3 (R^2 = 0.67), with low values occurring around 8:00 and 15:00 – 18:00, and high values at nighttime. Previous studies also showed that fossil fuel emissions could contribute 90% of the total NH_3 during haze days in urban Beijing (Pan et al., 2016). These results suggest that coal combustion could be an important source of NH_3 in urban Beijing. The similar diurnal trends of NH_3 and NH_4 indicated a regional transport characteristic for NH_x during this study. A great difference between the diurnal cycles of NH_3 and NH_x occurred during 8:00 – 16:00 when there was a negative correlation between f_{NH3} and NH_x due to the conversion of particle to gas.

3.2. Gas-particle partitioning of NH_x

In Fig. 3, during clean periods ($PM_1 \leq 17$ μg m^{-3}) NH_3 was about 8 μg m^{-3} (10 ppb). f_{NH3} correlated negatively with PM_1, indicating enhanced gas-to-particle conversion of NH_3 during high PM pollution situation (Figs. 3 and S3). Line A, Zones B, C and D were marked by dotted lines in Fig. 3. Line A illustrates the average background NH_3 concentration that appeared during clean days with strong northeast wind (Fig. 2), when NH_3 in Beijing during the winter season was mainly affected by emissions from regional agriculture and breeding industry of north China. NH_3 increased fast with the increase of PM_1 in Zone B ($17 < PM_1 \leq 125$ μg m^{-3}), indicating the linear and positive correlation with the accumulation of PM_1. Average NH_3 was relatively constant at an average (± 1σ) concentration of 17.0 ± 3.5 μg m^{-3} (or 22.8 ± 4.7 ppb) in Zone C ($125 < PM_1 \leq 272$ μg m^{-3}), and especially in zone D ($272 < PM_1 \leq 500$ μg m^{-3}). This is an indication that the basic NH_3 gas was still in excess relative to acidic gases (e.g., HNO_3 and HCl) during severe haze episodes.

There was a good exponential relationship between f_{NH3} and NH_4 (Fig. 4), as the R^2 and *Slope* between the measured and the reconstructed values of f_{NH3} were 0.92 and 0.99, respectively (Fig. S4).

Exponential relationships were usually observed between *T* and concentration of NH_3 (Aneja et al., 2000; Chang et al., 2015; Teng et al., 2017) as *T* is an important factor for gas-particle partitioning. The correlation between NH_3 and dew point (DP) was tightest among those of NH_3, NH_x, or NH_4 vs DP, RH, or *T* (Table S2). There was a border line of *T* at about 5 ℃, as high values of NH_4 and NH_3 appeared when $T < 5$ ℃ and $T > 5$ ℃, respectively (Fig. 5).

3.3. Potential sources and emission ratio (ER) for NH_x.

Considering the strong activity of gas-particle partitioning of NH_3, it is reasonable to detect the potential sources for NH_x instead of for NH_3 as NH_x approximately had a linear relationship with PM_1. The R^2 between the time series of tracers of potential sources and NH_3 and NH_x are presented in Table S3 for different time resolution (5 min, 6 h, and 1 day), in view of some instantaneous processes that might cause a delay in increase of NH_3, e.g., due to conversion to NH_4 through secondary aerosol formation. Tracers that had weak correlations with NH_3 and NH_x suggested insignificant contributions from the corresponding source, e. g., cooking was not an identified source of NH_x. In addition, NH_3 from traffic emission can vary not only between different running status of a car (Sun et al., 2014a), but also between different cars (Li et al., 2006). Hence, here we split the time series of NH_x into 35 segments to calculate the R^2 and slopes between the tracers and NH_x (Fig. S5).

CO, BC, and Chl correlated well with NH_x, with R^2 = 0.77, 0.72 and 0.68, respectively, suggesting that traffic and coal combustion were two significant sources of NH_x (Wang et al., 2015). Zhang et al. (2018) reported that local sources such as traffic emissions appeared to be important contributors to NH_3 in urban Beijing. CO_2 had relatively lower correlation with NH_x than CO did at

measurement time resolution of 5 min. Incomplete combustion of fossil fuels, e.g., cold start or low running speed of the car (Sun et al., 2014a), and charcoal barbecue or scattered coal burning (Li et al., 2016) usually caused spikes in the time series of CO. The R^2 between CO_2 vs NH_x was also lower than CO vs NH_x for lower time resolution of 6 hours or 1 day, indicating that incomplete combustion of fossil fuels was an important contributor to ER of NH_x. In view of the highly polluted surrounding areas (Wang et al., 2014), regional transport of NH_4 was likely a strong contributor to NH_x in Beijing. As the N fertilizer used in November and December were as low as ~ 2% of the whole year (Fu et al., 2015), and the NH_3 levels were correspondingly low in the two months (Damme et al., 2015) in the North China Plain, thus the agricultural emission from regional transport was unlikely an important source of NH_3 in Beijing during our study period.

NH_x correlated better with Aq-OOA (O:C = 0.82) and semi-volatile species such as particulate nitrate (R^2 = 0.83, and 0.88, respectively) than with the more oxidized OOA (O:C = 1.09) and SO_4 (R^2 = 0.58 and 0.81, respectively), appearing that local sources contributed more significantly to NH_x in urban Beijing. High correlation coefficients between O_3 and NH_x in our study were all observed during noon time (Fig. S5), e.g., in segments 6, 16, 20, 26, 32, 33, 35, when NH_x were also correlated well with BBOA, or FFOA. O_3 could be produced both from photochemical process and nighttime chemistry (Millet et al., 2016), and NH_3 was found to promote the generation of secondary organic aerosol (Huang et al., 2012; Na et al., 2006) during ozone-initiated reaction. Further research on the behavior of NH_x during atmospheric chemical reactions is still needed.

NH_x correlated best with CO among all primary tracers, thus CO was the most typical primary species for ER calculation of NH_x here. The high correlations of CO and NO_x (R^2 = 0.74) and vs Chl

(R^2 = 0.84) suggest that traffic and coal combustion were the major sources of CO in our study. The ER of [NH_x]/[CO] (ppbv/ppbv) ranged between 0.001 – 0.03 with a mean value of 0.011 (Table S4). The mean value was significantly lower than the ER of [NH_3]/[CO] (ppbv/ppbv) reported previously for traffic emissions (~ 0.03) (Sun et al., 2014a), and the automobiles and dairy facilities emission (~ 0.035) (Nowak et al., 2012). Biomass burning emissions and secondary formation also likely played a significant role for the high level of NH_x in Beijing as the ER of [NH_x]/[BBOA] (1.99 ppbv/μg m^{-3}) was higher than that of [NH_x]/[FFOA] (1.39 ppbv/μg m^{-3}), and the ER of [NH_x]/[OOA+aq-OOA] (3.86 ppbv/μg m^{-3}) was higher than that of [NH_x]/[FFOA+BBOA] (3.38 ppbv/μg m^{-3}).

Bivariate plots of NH_x (Fig. S6) show high concentration in the center area with low wind speed and also the south region with high wind speed, suggesting that the elevated NH_x concentration was mainly associated with local emissions and air masses transported from the south. Regional transport could also affect primary species, e.g., BBOA and Chl. The regional characteristics of NH_3 was unlikely caused by primary emissions, but rather due to the thermodynamics effect of the transported NH_4. The bivariate plot of f_{NH3} was similar to that of O_3, as both peaked when northwest wind prevailed. High NH_3 was mainly associated with east wind that resulted in high RH. The concentration of NH_x was low in the northwest direction due to less emission sources of pollutants, but there was an enhancement of the concentration of NH_3 in the farthest northwest direction under high wind speeds caused by the transport effect in clean situations. Sources of NO_2, SO_2, and OOA were mainly from the southwest, which was different with that of NH_x, indicating the weak contribution of these sources to NH_x. However, the distributions of the high concentrations of CO, NO, BC, Chl, FFOA, BBOA, and aq-OOA were generally within that of NH_x in Fig. S6, indicating similar source contributions for these species.

3.4. Vertical profiles of NH_3

The VPs_b_{ext} in this study (Fig. S7) were classified into four categories (Table S5) as discussed in detail in Wang et al. (2018), i.e., uniformly distributed (Fig. 6a), higher at lower heights caused by enhanced local emissions (Fig. 6b), higher aloft caused by regional transport (Fig. 6c), and significant transition caused by the formation of UBL (Fig. 6d). Mostly (87% of the time), the VPs_NH_3 were consistent with the VPs_b_{ext}. The vertical profiles of temperature in Fig. 6 followed the rules discussed in Wang et al. (2018). For example, there was no evident temperature inversion in Figs. 6a and b as the largest *T* inversion value was 0.2 ℃, but significant *T* inversion was found in Fig. 6c (3.3 ℃ at 80 m to 4.8℃ at 280 m) and d (3.0 ℃ at 80 m to 7.8 ℃ at 280 m). More detailed explanations for the four kinds of distinctive profiles can be found in Wang et al. (2018).

The 20th VP_b_{ext} (VP_b_{ext}_20) and VP_NH_3 (VP_NH_3_20) (Fig. S8 and Fig. 7a) were of a new kind of vertical profile, which decreased from 130 m to 170 m and increased above 170 m. As shown in Fig. S8, PM_1 during this vertical observation was increased from 106 μg m^{-3} at 6:05 to 112 μg m^{-3} at 7:05 at ground level with SNA (= sulfate+ nitrate + ammonium) accounting for about 35% of the PM_1 mass, and from 128 μg m^{-3} at 6:30 to 132μg m^{-3} at 6:41 at 260 m with SNA accounting for about 43%, indicating larger contribution of SNA and higher aerosol pollution level at 260 m. Small wind (~ 2 m s^{-1}) at the height range of 260 – 500 m was from the south during 6:30 – 8:00 (Figs. S8e and f), and *T* inversion occurred at about 80 m (Table S5), thus the shape of VP_b_{ext}_20 seemed to be a combination of the typical vertical profiles of III and IV in Figs. 6c and d, possibly caused by transport of pollutants from the south and/or the formation of low residual layer in the morning. Besides, the PM_1 at 260 m was rich in nitrate (~ 22% of PM_1), not in ammonium (~ 10% of PM_1),

thus, although the b_{ext} was increased by ~ 210 Mm^{-1} from 200 m to 235 m, the NH_3 was just increased by ~ 1ppb, indicating weak particle-to-gas partitioning of NH_x in case of the insufficient particle ammonium.

However, the vertical distribution of NH_3 showed a more homogeneous characteristic than those of b_{ext} below 260 m in general (Fig. S7), and occasionally, for 7% of the time, the VPs_NH_3 varied oppositely to the VPs_b_{ext}. VP_22_up ("up" means that the container was moving upward), VP_23_up (Fig. 7b) and VP_24 (Fig. 7c) were discussed here as the representative examples. The differences of RH and *T* between VP_22_up and VP_22_down ("down" means that the container was moving downward) were less than 5% and 0.5 ℃, respectively. The wind generally varied from east to south, indicating a similar meteorological condition for the two vertical profiles. PM_1 at ground level and 260 m was increased by 28 μg m^{-3} and 10 μg m^{-3} (Fig. S9), respectively. The contributions of NH_4 and NO_3 were generally constant at the two heights, and the increased contribution of SO_4 shall not promote the increase of NH_3, thus, the difference of NH_3 between VP_22_up and VP_22_down was probably due to the faster and direct emission of NH_3 from fossil fuel combustion at ground level as CO, CO_2 and NO_x in Fig. 2 all increased.

From VP_23_up to VP_23_down, PM_1 decreased by 32 μg m^{-3} at 260 m while increased by 91 μg m^{-3} at ground level (Fig. S9), indicating a strong accumulation of aerosol at ground level. Enhanced accumulation of NO_x, SO_2, and NO_z were also observed at ground level (Fig. 2). Thus, the variation of VP_NH_3_23_up was mainly caused by the enhanced local NH_3 emission, e. g., traffic emission and coal combustion. By contrast, the slower increase of VP_NH_3_23_down was generally driven by the enhanced consumption of NH_3 due to gas-to-particle partitioning at high level of RH (≈

70%) as the f_{NH3} was larger (Fig. 2). The UBL was confined to below 200 m during VP_23_down. RH was increased by ~ 10%, *T* was decreased by ~ 1 ℃ below 200 m, which would facilitate the formation of NH_4, but it played a much weaker role on NH_3 than on aerosol as the vertical differences of VP_NH_3_23_down and VP_b_{ext}_23_down were 8% and 32%, respectively.

For VP_24, *T* inversion occurred at about 150 m when b_{ext} gradually decreased with the height, indicating the formation of low UBL. PM_1 at 260 m was decreased by only ~ 2% (from 292 μg m^{-3} to 286 μg m^{-3}), and at ground level was by about 8% (from 433 μg m^{-3} to 467 μg m^{-3}) (Fig. S9) from VP_24_up to VP_24_down. VP_b_{ext}_24 was of the type IV in Fig. 6d, but the trend of VP_NH_3 was totally an opposite. One explanation was that, at such high level of PM and RH (≈ 95%) below 200 m, NH_3 was mainly determined by gas-particle partitioning balance affected by both of the temperature and aerosol chemical composition, as to maintain an ion balance, it still needed NH_4 (= SO_4/96×2×18 + NO_3/62×18 + Chl/35.5×18 - NH_4) of about 35 μg m^{-3} and 20 μg m^{-3}, respectively at ground level and 260 m, thus NH_3 was greatly consumed to provide NH_4. It is consistent with that particle is acidic during winter haze episodes (Guo et al., 2017; Liu et al., 2017). Later, higher temperature and lower aerosol mass concentration for VP_24_up caused higher values of NH_3 than that for VP_24_down.

3.5. The vertical difference between NH_3 and particles

In Fig. 8, all the data points measured during the vertically resolved experiments fell in the region defined by measurements from the ground level, indicating similar evolution mechanism of NH_3 versus b_{ext} below 260 m. The data points measured during each vertically resolved experiment were usually clustered due to the uniform vertical distribution of NH_3 concentration. Compared with

the relationship between VP_NO_2 vs VP_b_{ext} reported in Wang et al. (2018), VP_NH_3 increased faster with VP_b_{ext} and NH_3 had a maximum value of about 35 ppb in the b_{ext} range of 0 – 2000 Mm^{-1}. In Fig. 9a, both b_{ext} and NH_3 were higher during nighttime due to lower UBL, as well as enhanced coal heating and truck emissions. The diurnal variation (= (nighttime- daytime)/whole campaign) of average VP_NH_3 and VP_b_{ext} in Fig. 9a are 0.13 and 0.93 respectively, indicating much smaller diurnal variation of VP_NH_3 below 260 m, which supports the result that NH_3 is rich below 260 m. The comparison between diurnal variation of average VP_NH_3 and VP_b_{ext} were shown in Fig. 9b. Regional transport and the formation of residual layer above 200 m caused higher values above 200 m during nighttime of VP_b_{ext} and VP_NH_3. Low UBL height at nighttime resulted in the decrease in VP_b_{ext} below 200 m, however, the VP_NH_3 showed an opposite trend mainly due to the gas-to-particle partitioning of NH_x. For instance, more NH_3 was needed to form ammonium salt at ground level as 13 μg m^{-3} of NH_4 was in shortage to maintain ion balance, higher than that during daytime (6 μg m^{-3}) and at 260 m (3 – 8 μg m^{-3}). The nocturnal NH_3/b_{ext} was smaller than the diurnal NH_3/b_{ext}, it was partly caused by large values of NH_3/b_{ext} in clean periods (Fig. S7) that usually appeared during daytime, e. g., the NH_3/b_{ext} of VPs_9 – 12, VP_15, and VP_16 were in the range of 250 – 1600 ppt/Mm^{-1}, and the lower *T* and higher RH (Fig. S10) during nighttime that facilitated the gas-to-particle partitioning of NH_x.

In Fig. S11, most VPs_b_{ext} decreased with height, however, about half of VPs_NH_3 showed opposite trend. 96% of the vertical variation (the ratios of one standard deviation to mean value (Sdev/Avg), (Max-Min)/(2×Avg)) of NH_3 were smaller than that of b_{ext}. The average value of Sdev/Avg of VP_b_{ext} was about 4 times of that of VP_NH_3, proving, once again, the much more homogeneous vertical distribution of NH_3 in urban area in Beijing below 260 m.

In Fig. 10, the ratios of PM_1 and NH_4 at 260 m to ground level were 1.35 and 1.25, respectively, whereas, the ratios for NH_3 and f_{NH3} were very close to 1 (0.98 and 0.93, respectively; Fig. 10c and d). Moreover, NH_3 concentration correlated better between the two heights (R^2 = 0.88; Fig. 10c) than PM_1 or NH_4 (R^2 = 0.81 for both; Fig. 10a and b) also suggested a more homogeneous mixing of NH_3. The exponential relationships between NH_3 vs. PM_1 and f_{NH3} vs. NH_4 were very similar between ground level and 260 m (Fig. 11), indicating similar gas-particle partitioning mechanisms below 260 m. The small difference of DP between 8 m and 280 m (approximately 2 ℃ in this study; Fig. S12a) might be a reason for this similar gas-particle partitioning mechanism.

Besides, SO_2 and CO at 260 m correlated well with those at ground level (R^2 = 0.57 and 0.63, respectively), indicating similar combustion sources for NH_x within 260 m (Fig. S13a). The average ratios of SO_2 and CO at ground level to those at 260 m were 0.7 and 1.1, respectively. It is reasonable that coal combustion for residential heating has been well controlled in urban Beijing, and SO_2 emitted from coal combustion was more likely from surrounding areas, especially during night time (Fig. S13b). Comparatively, CO was generally higher at ground level than 260 m due to the influence of traffic emissions in urban Beijing.

4. Conclusions and implications

The average NH_3 concentration was 12.3 μg m^{-3} (16.5 ppb) in winter in Beijing, lower than those reported in tunnel studies and in summer in rural Beijing. NH_3 remained constant during both clean periods (PM_1 < 17 μg m^{-3}) and heavily polluted episodes (PM_1 > 272 μg m^{-3}), with average concentration at about 8 μg m^{-3} and 17 μg m^{-3}, respectively. Gas-particle partitioning played less distinctive role in controlling NH_3 during periods with PM_1 ranging from 17 to 125 μg m^{-3} (NH_3 = 8 – 16 μg m^{-3}) when NH_3 correlated positively and linearly with PM_1. NH_x in Beijing came from

complex sources. Primary emissions of biomass burning, coal combustion, and traffic were three significant contributors to NH_x. The regional transport was also a strong contribution to NH_x as it correlated well with secondary species, e.g., aq-OOA, NO_3, and SO_4. The average wind speed was usually about 5 m s^{-1} at the height of 280 m, thus the pollutants from surrounding areas within about 400 km, e.g., Hebei (Wang et al., 2014) and Shandong Provinces (Wang et al., 2016), could arrive at Beijing in one day. Once the exact sources for NH_x had been resolved, the source contributions for NH_3 could be reconstructed according to the good exponential relationship between f_{NH3} and NH_4.

Vertically resolved measurements also showed four types of vertical profiles for b_{ext}, which were associated with well mixed atmosphere, fast accumulation of local emissions, regional transport aloft, and the formation of low urban boundary layer, consistent with those reported in Wang et al. (2018). The vertical distribution of NH_3 was generally consistent with that of b_{ext}, but was more homogeneous due to the stronger diffusivity of NH_3. The strong gas-particle partitioning effect associated with high contribution of sulfate, nitrate and chloride was an important reason for the different vertical distributions between NH_3 and b_{ext} during high PM pollution situation. The formation of UBL played a much weaker role on NH_3 than on aerosol, just when both the strong temperature inversion and large aerosol gradient occurred, the formation of UBL shall play a significant role on the vertical profiles of NH_3 below 260 m, e. g. VP_25 (Fig. 6d).

Appendix A. Supplementary material

Supplementary Information accompanies this paper (Figs. S1-S12, Tables S1-S5) including detailed description of the data quality, methodology, bivariate polar plots of pollution species, correlations between pollution species, aerosol chemical compositions, and information of vertical

profiles of NH_3 and b_{ext}.

Acknowledgements

This work was supported by the National Postdoctoral Program for Innovative Talents (BX201600157), the General Financial Grant from the China Postdoctoral Science Foundation (2017M610972), the National Natural Science Foundation of China (41705115) and the UK Natural Environment Research Council (NERC; NE/N006992/1).

Notes

The authors declare no competing financial interest.

References

Aneja, V.P., Chauhan, J.P., Walker, J.T., 2000. Characterization of atmospheric ammonia emissions from swine waste storage and treatment lagoons. J. Geophys. Res. 105, 11535–11545.

Baer, D.S., Paul, J.B., Gupta, M., O'Keefe, A., 2002. Sensitive absorption measurements in the near-infrared region using off-axis integrated-cavity-output spectroscopy. Appl. Phys. B: Lasers and Optics 75, 261-265.

Chang, Y.H., Zou, Z., Deng, C.R., Huang, K., Collett, J.L., Jr., Lin, J., Zhuang, G.S., 2015. The importance of vehicle emissions as a source of atmospheric ammonia in the megacity of Shanghai. Atmos. Chem. Phys. 15, 34719-34763.

Damme, M. V., Erisman, J. W., Clarisse, L., Dammers, E., Whitburn, S., Clerbaux, C., Dolman A. J., Coheur P. F., 2015. Worldwide spatiotemporal atmospheric ammonia (NH_3) columns variability revealed by satellite. Geophys. Res. Lett. 42, 8660–8668, doi:10.1002/2015GL065496.

Elser, M., El-Haddad, I., Maasikmets, M., Bozzetti, C., Wolf, R., Ciarelli, G., Slowik, J.G., Richter,

R., Teinemaa, E., Hüglin, C., 2018. High contributions of vehicular emissions to ammonia in three European cities derived from mobile measurements. Atmos. Environ. 210-220.

Fu, X., Wang, S. X., Ran, L. M., Pleim, J. E., Cooter, E., Bash, J. O., Benson V., Hao J. M., 2015. Estimating NH_3 emissions from agricultural fertilizer application in china using the bi-directional cmaq model coupled to an agro-ecosystem model. Atmos. Chem. Phys. 15(1), 745-778.

Giannadaki, D., Giannakis, E., Pozzer, A., Lelieveld, J., 2018. Estimating health and economic benefits of reductions in air pollution from agriculture. Sci. Total Environ. 622-623, 1304-1316.

Guo, H., Liu, J., Froyd, K.D., Roberts, J.M., Veres, P.R., Hayes, P.L., Jimenez, J.L., Nenes, A., Weber, R.J., 2017. Fine particle pH and gas–particle phase partitioning of inorganic species in Pasadena, California, during the 2010 CalNex campaign. Atmos. Chem. Phys. 17, 5703-5719.

Guo, H., Otjes, R., Schlag, P., Kiendler-Scharr, A., Nenes, A., Weber, R.J., 2018. Effectiveness of ammonia reduction on control of fine particle nitrate. Atmos. Chem. Phys. 18, 12241-12256.

Huang, Y., Lee, S.C., Ho, K.F., Ho, S.S.H., Cao, N., Cheng, Y., Gao, Y., 2012. Effect of ammonia on ozone-initiated formation of indoor secondary products with emissions from cleaning products. Atmos. Environ. 59, 224-231.

Li, Q., Jiang, J., Cai, S., Zhou, W., Wang, S., Duan, L., Hao, J., 2016. Gaseous Ammonia Emissions from Coal and Biomass Combustion in Household Stoves with Different Combustion Efficiencies. Environ. Sci. Technol. Lett. 3, 98-103.

Li, Y., Schwab, J.J., Demerjian, K.L., 2006. Measurements of ambient ammonia using a tunable diode laser absorption spectrometer: Characteristics of ambient ammonia emissions in an urban area of New York City. J. Geophys. Res. 111, 1599-1609.

Liu, M., Song, Y., Zhou, T., Xu, Z., Yan, C., Zheng, M., Wu, Z., Hu, M., Wu, Y., Zhu, T., 2017. Fine particle pH during severe haze episodes in northern China. Geophys. Res. Lett. 44, 5213-5221.

Liu, T., Wang, X., Wang, B., Ding, X., Deng, W., Lü, S., Zhang, Y., 2014. Emission factor of ammonia (NH3) from on-road vehicles in China: tunnel tests in urban Guangzhou. Environ. Res. Lett. 9, 064027.

Liu, X., Cheng, X., Hu, F., 2015. Gradient characteristics of CO2 concentration and flux in Beijing urban area part I: Concentration and virtual temperature. Chinese J. Geophys. (in Chinese) 58, 1502-1512.

Meng, Z., Xu, X., Lin, W., Ge, B., Xie, Y., Song, B., Jia, S., Zhang, R., Peng, W., Wang, Y., Cheng, H., Yang, W., Zhao, H., 2018. Role of ambient ammonia in particulate ammonium formation at a rural site in the North China Plain. Atmos. Chem. Phys. 18, 167-184.

Millet, D.B., Baasandorj, M., Hu, L., Mitroo, D., Turner, J., Williams, B.J., 2016. Nighttime Chemistry and Morning Isoprene Can Drive Urban Ozone Downwind of a Major Deciduous Forest. Environ. Sci. Technol. 50, 4335-4342.

Na, K., Song, C., Iii, D.R.C., 2006. Formation of secondary organic aerosol from the reaction of styrene with ozone in the presence and absence of ammonia and water. Atmos. Environ. 40, 1889-1900.

Nowak, J.B., Neuman, J.A., Bahreini, R., Middlebrook, A.M., Holloway, J.S., Mckeen, S.A., Parrish, D.D., Ryerson, T.B., Trainer, M., 2012. Ammonia sources in the California South Coast Air Basin and their impact on ammonium nitrate formation. Geophys. Res. Lett. 39, 102-114.

Pan, Y., Tian, S., Liu, D., Fang, Y., Zhu, X., Gao, M., Gao, J., Michalski, G., Wang, Y., 2018. Isotopic evidence for enhanced fossil fuel sources of aerosol ammonium in the urban atmosphere.

Environ. Pollut. 238, 942–947.

Pan, Y., Tian, S., Liu, D., Fang, Y., Zhu, X., Zhang, Q., Zheng, B., Michalski, G., Wang, Y., 2016. Fossil Fuel Combustion-Related Emissions Dominate Atmospheric Ammonia Sources during Severe Haze Episodes: Evidence from 15N-Stable Isotope in Size-Resolved Aerosol Ammonium. Environ. Sci. Technol. 50, 8049-8056.

Pozzer, A., Tsimpidi, A.P., Karydis, V.A., de Meij, A., Lelieveld, J., 2017. Impact of agricultural emission reductions on fine-particulate matter and public health. Atmos. Chem. Phys. 17, 12813-12826.

Shen, J., Liu, X., Zhang, Y., Fangmeier, A., Goulding, K., Zhang, F., 2011. Atmospheric ammonia and particulate ammonium from agricultural sources in the North China Plain. Atmos. Environ. 45, 5033-5041.

Sun, K., Tao, L., Miller, D.J., Khan, M.A., Zondlo, M.A., 2014a. On-Road Ammonia Emissions Characterized by Mobile, Open-Path Measurements. Environ. Sci. Technol. 48, 3943.

Sun, Y., Jiang, Q., Wang, Z., Fu, P., Li, J., Yang, T., Yin, Y., 2014b. Investigation of the sources and evolution processes of severe haze pollution in Beijing in January 2013. J. Geophys. Res. 119, 4380-4398.

Sun, Y., Wang, Z., Dong, H., Yang, T., Li, J., Pan, X., Chen, P., Jayne, J.T., 2012. Characterization of summer organic and inorganic aerosols in Beijing, China with an Aerosol Chemical Speciation Monitor. Atmos. Environ. 51, 250-259.

Sun, Y., Wang, Z., Fu, P., Yang, T., Jiang, Q., Dong, H., Li, J., Jia, J., 2013. Aerosol composition, sources and processes during wintertime in Beijing, China. Atmos. Chem. Phys. 13, 4577-4592.

Sun, Y., Wei, D., Wang, Q., Zhang, Q., Chen, C., Chen, Y., Chen, Z., Fu, P., Wang, Z., Gao, Z., 2015.

Real-Time Characterization of Aerosol Particle Composition above the Urban Canopy in Beijing: Insights into the Interactions between the Atmospheric Boundary Layer and Aerosol Chemistry. Environ. Sci. Technol. 49, 11340-11347.

Teng, X., Hu, Q., Zhang, L., Qi, J., Shi, J., Xie, H., Gao, H., Yao, X., 2017. Identification of Major Sources of Atmospheric NH3 in an Urban Environment in Northern China During Wintertime. Environ. Sci. Technol. 51, 6839.

Tevlin, A.G., Li, Y., Collett, J.L., McDuffie, E.E., Fischer, E.V., Murphy, J.G., 2017. Tall Tower Vertical Profiles and Diurnal Trends of Ammonia in the Colorado Front Range. J. Geophys. Res. 122, 12468-12487.

Van Damme, M., Clarisse, L., Whitburn, S., Hadji-Lazaro, J., Hurtmans, D., Clerbaux, C., Coheur, P.-F., 2018. Industrial and agricultural ammonia point sources exposed. Nature 564, 99-103.

Wang, L., Wei, Z., Yang, J., Zhang, Y., Zhang, F., Su, J., Meng, C., Zhang, Q., 2014. The 2013 severe haze over the southern Hebei, China: model evaluation, source apportionment, and policy implications. Atmos. Chem. Phys. 14, 3151-3173.

Wang, Q., Sun, Y., Jiang, Q., Du, W., Sun, C., Fu, P., Wang, Z., 2015. Chemical composition of aerosol particles and light extinction apportionment before and during heating season in Beijing, China. J. Geophys. Res. 120, 12708-12722.

Wang, Q., Sun, Y., Xu, W., Du, W., Zhou, L., Tang, G., Chen, C., Cheng, X., Zhao, X., Ji, D., Han, T., Wang, Z., Li, J., Wang, Z., 2018. Vertically resolved characteristics of air pollution during two severe winter haze episodes in urban Beijing, China. Atmos. Chem. Phys. 18, 2495-2509.

Wang, S., Xing, J., Jang, C., Zhu, Y., Fu, J.S., Hao, J., 2011. Impact Assessment of Ammonia Emissions on Inorganic Aerosols in East China Using Response Surface Modeling Technique.

Environ. Sci. Technol. 45, 9293-9300.

Wang, Y., Bao, S., Wang, S., Hu, Y., Shi, X., Wang, J., Zhao, B., Jiang, J., Zheng, M., Wu, M., 2016. Local and regional contributions to fine particulate matter in Beijing during heavy haze episodes. Sci. Total Environ. 580, 283-296.

Xu, W., Sun, Y., Wang, Q., Zhao, J., Wang, J., Ge, X., Xie, C., Zhou, W., Du, W., Li, J., Fu, P., Wang, Z., Worsnop, D.R., Coe, H., 2018. Changes in Aerosol Chemistry from 2014 to 2016 in Winter in Beijing: Insights from High Resolution Aerosol Mass Spectrometry. J. Geophys. Res. 124, 1132-1147.

Zhang, J.K., Wang, Y.S., Huang, X.J., Liu, Z.R., Ji, D.S., Sun, Y., 2015. Characterization of organic aerosols in Beijing using an aerodyne high-resolution aerosol mass spectrometer. Adv. Atmos. Sci. 32, 877-888.

Zhang, X., Wu, Y., Liu, X., Reis, S., Jin, J., Dragosits, U., Van, D.M., Clarisse, L., Whitburn, S., Coheur, P.F., 2017. Ammonia emissions may be substantially underestimated in China. Environ. Sci. Technol. 51, 12089-12096.

Zhang, Y., Tang, A., Wang, D., Wang, Q., Benedict, K., Zhang, L., Liu, D., Li, Y., Collett Jr, J.L., Sun, Y., Liu, X., 2018. The vertical variability of ammonia in urban Beijing, China. Atmos. Chem. Phys. 18, 16385-16398.

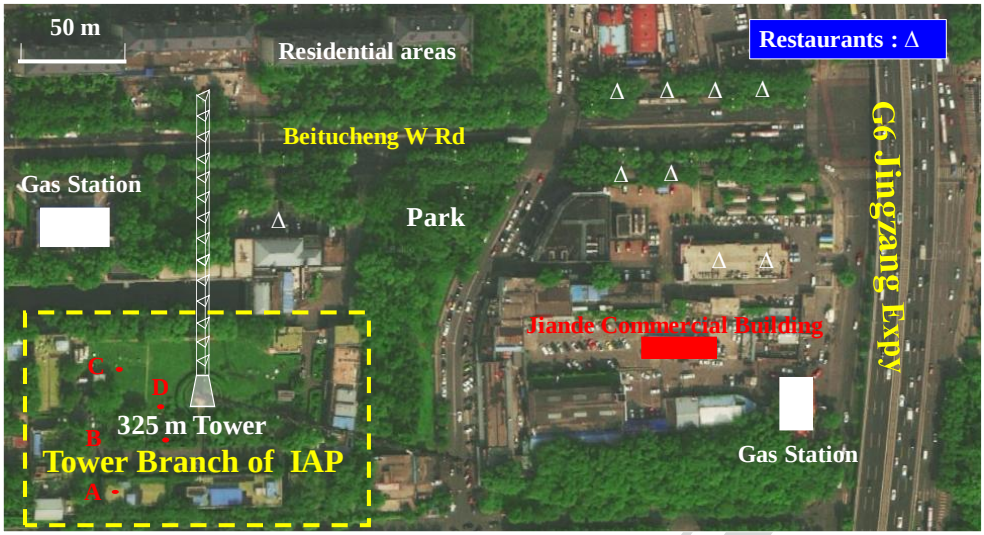

Fig. 1. Sampling site and its surroundings.

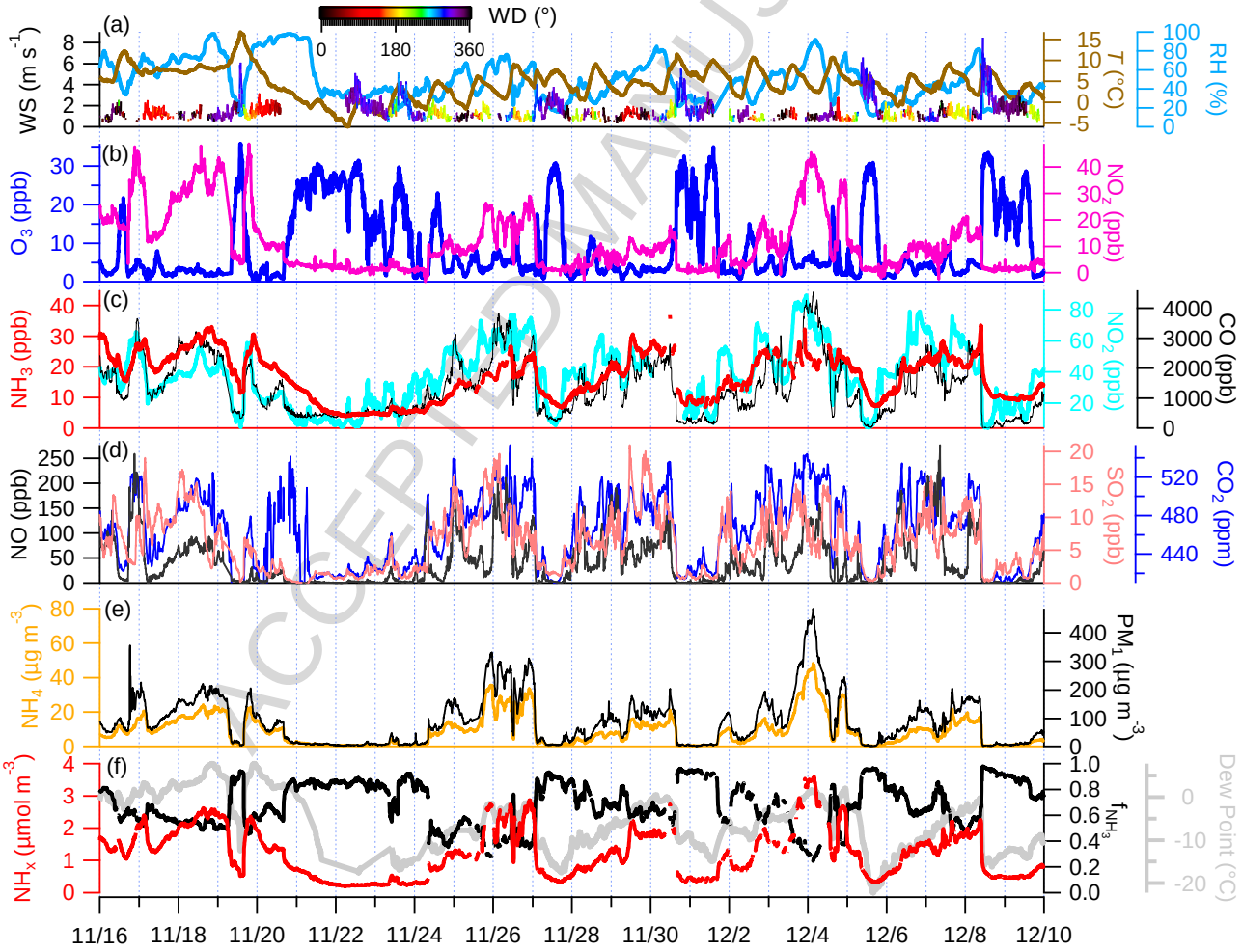

Fig. 2. Time series of (a) WS, WD, RH, and *T*; (b) O_3 and NO_z; (c) NH_3, NO_2, and CO; (d) NO,

SO_2, and CO_2; mass concentrations of (e) NH_4 and PM_1; (f) molar concentration of NH_x, f_{NH3}, and dew point at the ground level of TBIAP (39°58′N, 116°22′E; elevation: 49 m ASL).

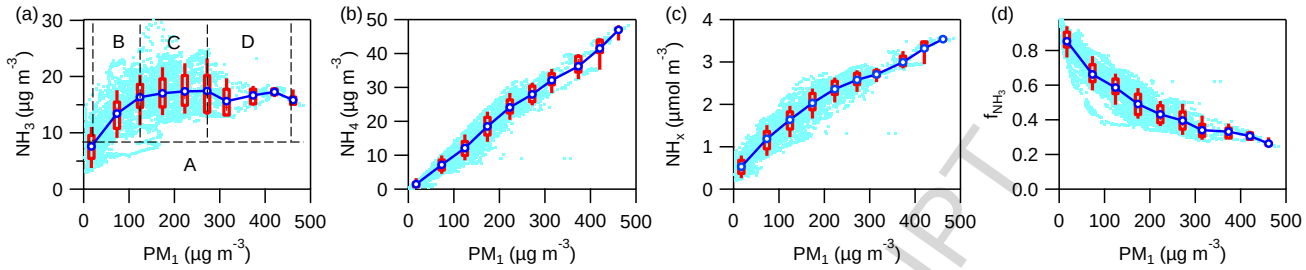

Fig. 3. Variations of (a) NH_3, (b) NH_4, (c) NH_x, and (d) f_{NH3} as a function of PM_1 mass concentration with the boxes showing the mean (blue circles), median, 10th, 25th, 75th and 90th percentiles of the data values.

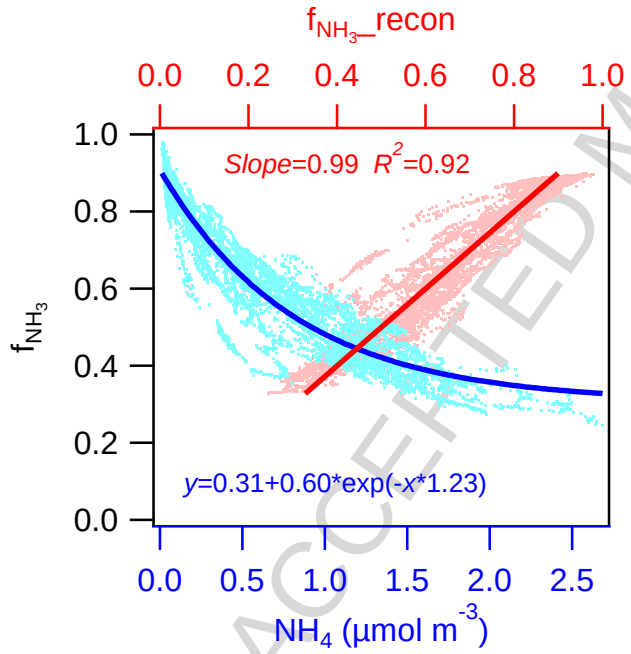

Fig. 4. Relationships between f_{NH3} and NH_4, and between measured and reconstructed f_{NH3} with NH_4.

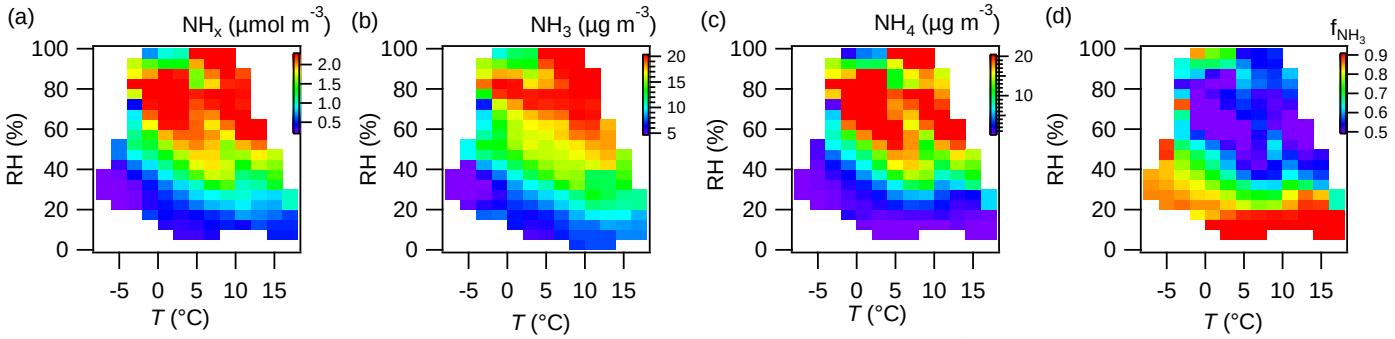

Fig. 5. RH and *T* dependence of (a) molar concentration of NH_x, mass concentration of (b) NH_3 and (c) NH_4, and (d) f_{NH3}.

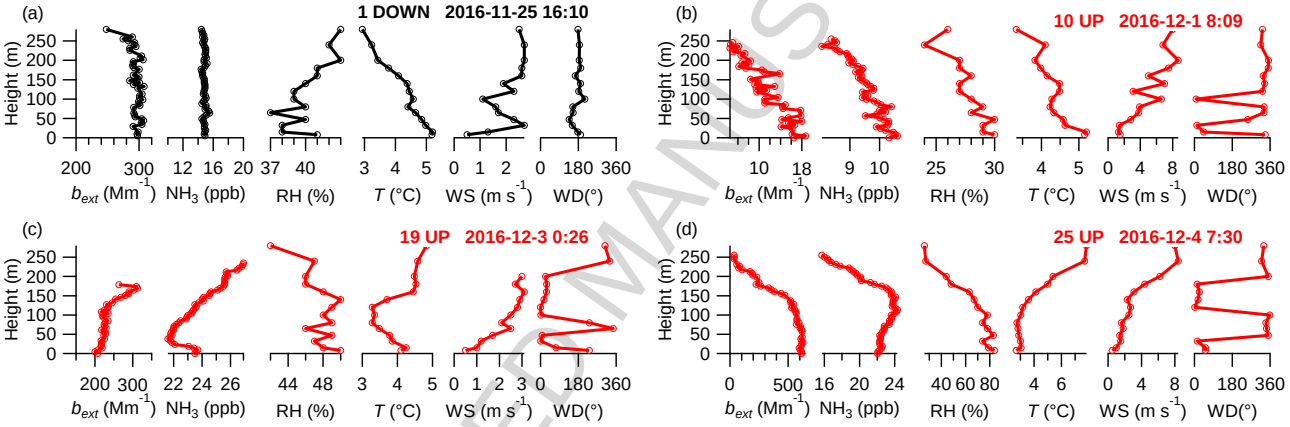

Fig. 6. Examples for four typical types of VP_NH_3 which are consistent with of VP_b_{ext} according to the results reported in Wang et al. (2018), together with the corresponding vertical profiles of RH, WD, WS, and *T*. The serial number of the vertically resolved experiments were added in each figure, and the moving directions of the container were marked in red (UP) and black (DOWN) color, respectively.

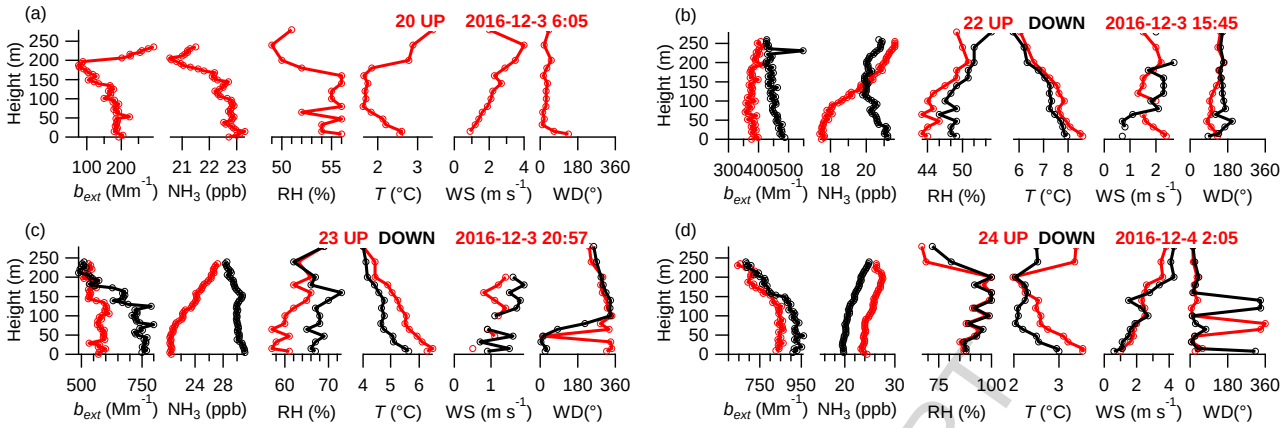

Fig. 7. The typical types of VP_NH_3 that could not be classified with the method in Wang et al. (2018), together with the corresponding vertical profiles of b_{ext}, RH, and T. The serial number of the vertically resolved experiments were added in each figure, and the moving directions of the container were marked in red (UP) and black (DOWN) color for the vertical profiles, respectively.

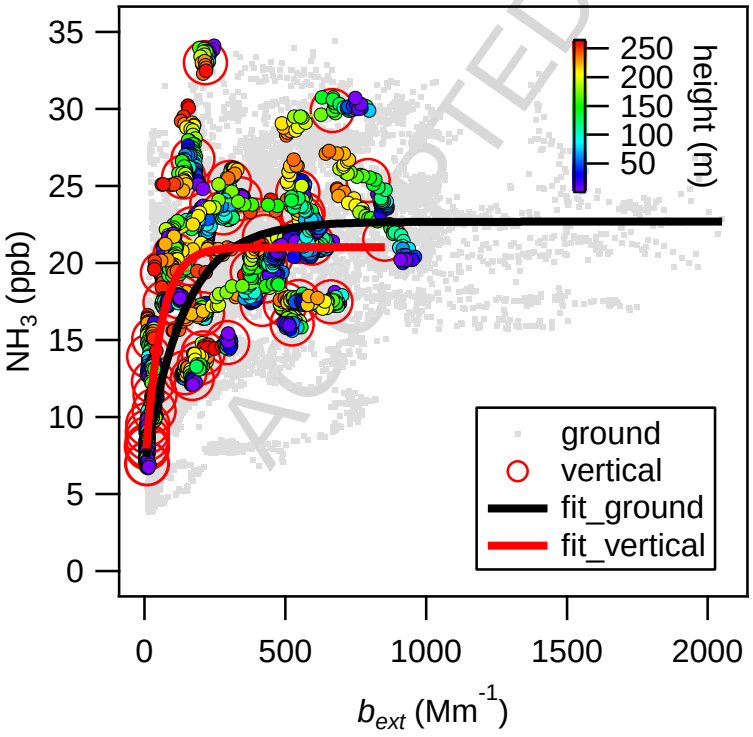

Fig. 8. Comparison of NH_3 vs b_{ext} measured at ground level (gray points) and during vertically

resolved measurements (round points colored by heights were measured during each vertically resolved measurement, red circles are the average values for each vertically resolved measurement.

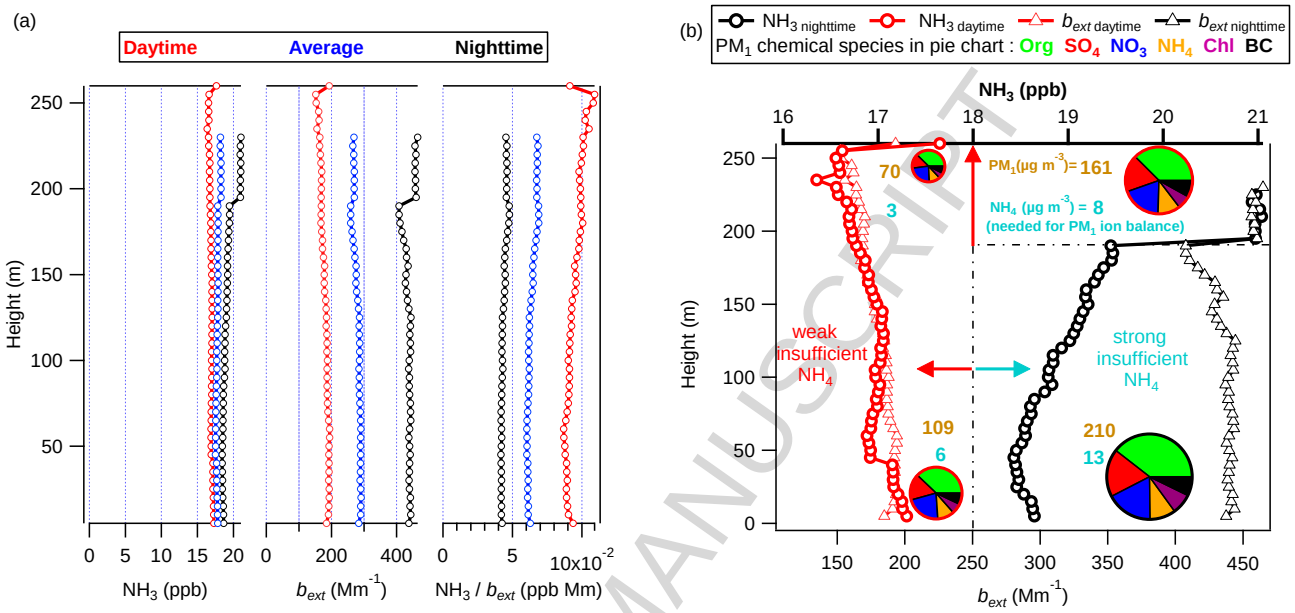

Fig. 9. Average vertical distribution of (a) b_{ext}, NH_3, and NH_3/b_{ext} for all data points, and for data points that during daytime and nighttime, respectively. (b) Comparison of vertical distribution of NH_3 vs b_{ext} measured during daytime and nighttime and the corresponding PM chemical composition at 260 m and ground level.

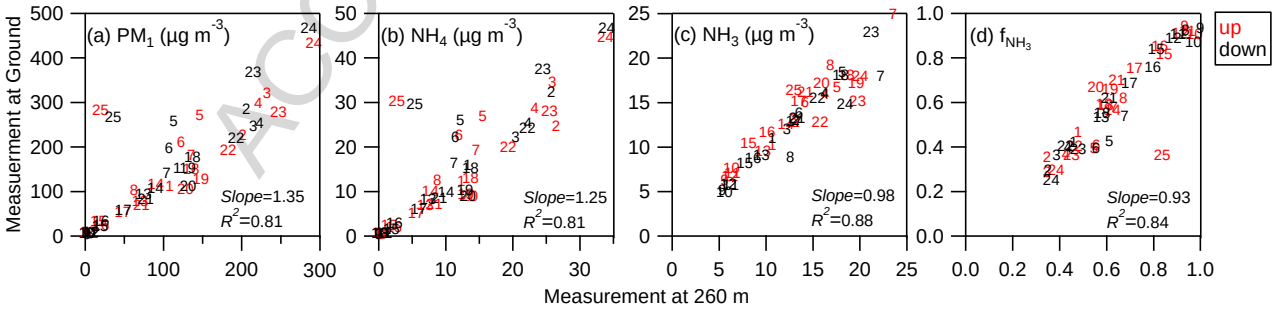

Fig. 10. Comparisons of (a) PM_1, (b) NH_4, (c) NH_3 and (d) f_{NH3} between 260 m and ground level. Data points were marked by the serial number of the experiments (Fig. S7). Data points

measured for up and down experiments were marked in red and black color, respectively. Data points for down experiment 14, 19, 20, and 25 were not used for calculation of R^2 and *Slope* due to the incomplete measurement of VP_NH_3. NH_3 measured at 240 m during nighttime was approximately used as the value at 260 m as the moving time from 240 m to 260 m is about 2.5 minutes (=20/8min).

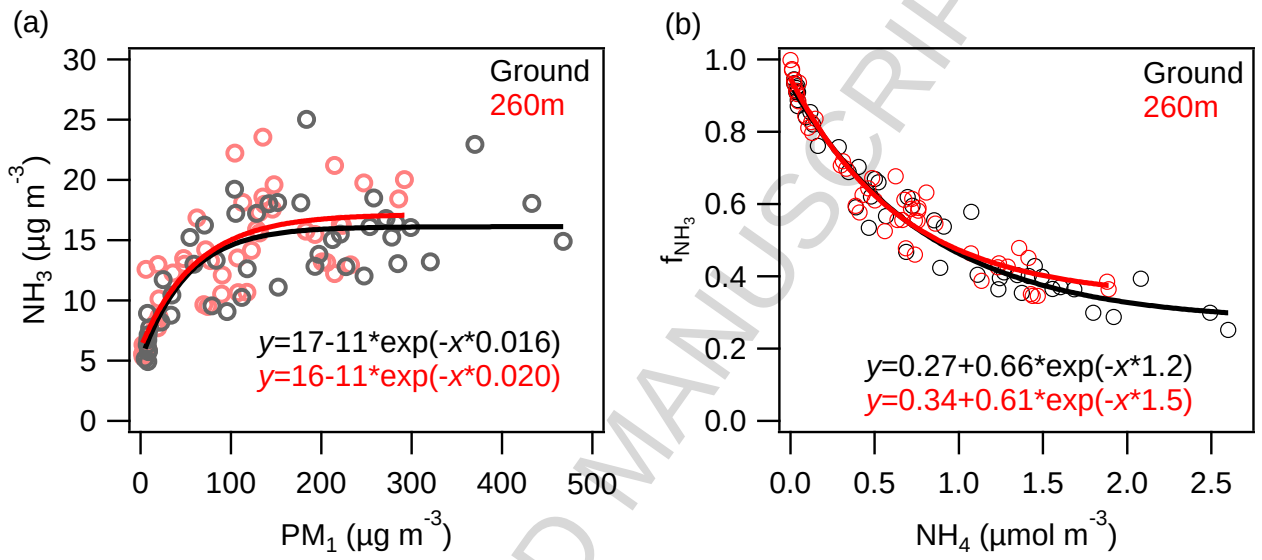

Fig. 11. (a) Variations of NH_3 as a function of PM_1 mass concentration, and (b) relationship between f_{NH3} and NH_4 concentration at ground level (black circles) and 260 m (red circles) during the vertically resolved experiments.

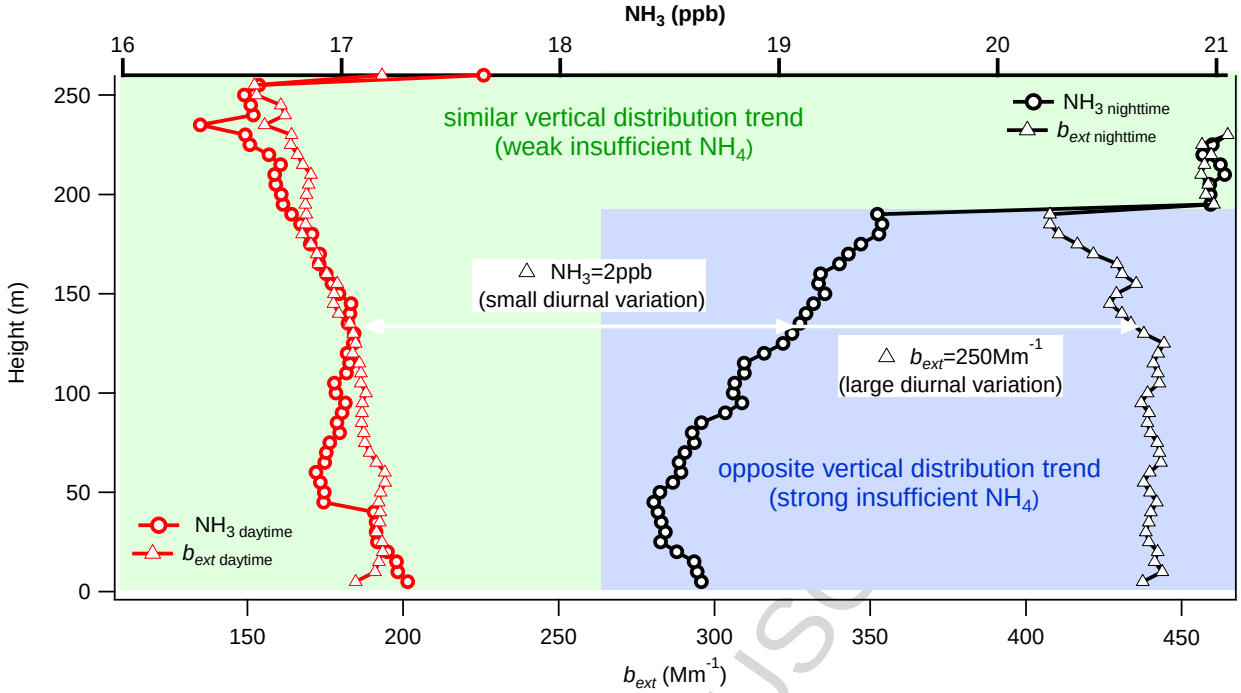

Graphical abstract

HIGHLIGHTS

Gas-particle partitioning plays a significant role on NH_3 concentration.
NH_3 remains relatively constant at high PM and NH_4 levels.
Gas-to-particle partitioning can cause opposite vertical profiles of NH_3 and b_{ext}.
Vertical distribution of NH_3 is more homogeneous than that of b_{ext}